

A connection between Scott-Vogelius and grad-div stabilized Taylor-Hood FE approximations of the Navier-Stokes equations

Michael A. Case* Vincent J. Ervin† Alexander Linke ‡
Leo G. Rebholz§

Abstract

This article studies two methods for obtaining excellent mass conservation in finite element computations of the Navier-Stokes equations using continuous velocity fields. With a particular mesh construction, the Scott-Vogelius element pair has recently been shown to be inf-sup stable and have optimal approximation properties, while also providing pointwise mass conservation. We present herein the first numerical tests of this element pair for the time dependent Navier-Stokes equations. We also prove that the limit of the grad-div stabilized Taylor-Hood solutions to the Navier-Stokes problem converges to the Scott-Vogelius solution as the stabilization parameter tends to infinity. That is, we provide theoretical justification that choosing the grad-div parameter large does not destroy the solution. Numerical tests are provided which verify the theory, and show how both Scott-Vogelius and grad-div stabilized Taylor-Hood (with large stabilization parameter) elements can provide accurate results with excellent mass conservation for Navier-Stokes approximations.

1 Introduction

This article studies two finite element methods for approximating solutions to the Navier-Stokes equations (NSE) that use continuous velocity fields and provide accurate approximations as well as excellent mass conservation. Under the restriction that the mesh be created as a barycenter refinement of a triangular/tetrahedral mesh, and that the degree k of approximating polynomial for velocity be chosen at least as large as the dimension of the domain space, $k \geq d$, the $((P_k)^d, P_{k-1}^{disc})$ pair (called the Scott-Vogelius (SV) pair [40, 39, 35, 36]), has recently been shown to be inf-sup stable and admit optimal approximation properties [43, 42, 31, 1]. If $d = 3$ and $k = 2$, these properties also hold provided a Powell-Sabin tetrahedral mesh is used (described in Section 2) [44]. The SV pair has the fundamental physical property that, since $\nabla \cdot (P_k)^d \subset P_{k-1}^{disc}$, the weak enforcement of mass

*Department of Mathematical Sciences, Clemson University, Clemson, SC 29634, mcase@clemson.edu. Partially supported by National Science Foundation grant DMS0914478.

†Department of Mathematical Sciences, Clemson University, vjervin@clemson.edu, <http://www.math.clemson.edu/~vjervin>.

‡Weierstrass Institute for Applied Analysis and Stochastics, Mohrenstr. 39, 10117 Berlin Germany, linke@wias-berlin.de, <http://www.wias-berlin.de/people/linke>

§Department of Mathematical Sciences, Clemson University, Clemson, SC 29634, rebholz@clemson.edu, <http://www.math.clemson.edu/~rebholz>. Partially supported by National Science Foundation grant DMS0914478.

conservation imposed by the usual Galerkin finite element method for Stokes or the NSE actually enforces strong (pointwise) conservation of mass.

The second method studied herein is the Galerkin method for the NSE with Taylor-Hood (TH) elements and grad-div stabilization (with parameter γ). This method is well studied in the general case [28, 30, 8, 19], and it is well known that the stabilization improves mass conservation and relaxes the effect of the pressure error on the velocity error. We show that under conditions where SV elements are LBB stable, the TH solutions corresponding to a sequence of grad-div parameters $\gamma_n \rightarrow \infty$ converge to the SV solution. This provides theoretical justification that one can choose γ significantly larger than $O(1)$ (see [8, 26]), and still obtain an accurate solution with excellent mass conservation, although computationally care for numerical roundoff error still must be taken. We also prove that on a regular mesh, as $\gamma_n \rightarrow \infty$ the TH solutions converge to a solution which is also pointwise mass conservative.

Although the incompressible NSE are one of the most investigated mathematical equations [37, 38, 18, 12, 15, 9, 13, 4, 11, 33, 6], their numerical solution remains a difficult challenge, and new methods and strategies for their solution are regularly proposed. Nevertheless, even in the case of laminar, single phase Newtonian fluids, some important aspects of their numerical approximation are sometimes overlooked, such as the importance of mass conservation [30, 7, 23, 8, 26, 21, 22]. It is well-known that mixed finite element discretizations of the incompressible NSE are prone to different kinds of numerical instabilities, when one combines a certain discrete velocity space X_h in a naive way with a discrete pressure space Q_h . The violation of discrete inf-sup stability [4, 9, 33] is the classical example for when the discrete pressure space is too large in relation to the discrete velocity space. The opposite extreme is when the discrete pressure space is too small. In this case the approximation does not adequately satisfy the conservation of mass equation, thereby giving a poor approximation to the physical solution. To illustrate this instability, consider the following linear steady Stokes problem in \mathbb{R}^2 , $\Omega = (0, 1) \times (0, 1)$:

$$\begin{aligned} -\Delta \mathbf{u} + \nabla p &= \text{Ra} \begin{bmatrix} 0 \\ y \end{bmatrix}, \text{ in } \Omega, \\ \nabla \cdot \mathbf{u} &= 0, \text{ in } \Omega, \\ \mathbf{u} &= \mathbf{0}, \text{ on } \partial\Omega. \end{aligned}$$

This problem is derived from Rayleigh-Bénard convection with Boussinesq approximation [24] at large Prandtl numbers. It models the system behavior before there is an onset of convection, and heat transfer is only conductive and a linear function of y . In this case, the typical Rayleigh number Ra is of order 10^8 and the fluid does not move, i.e., the obvious (mean pressure = 0) solution of the problem is $(\mathbf{u}, p) = (\mathbf{0}, \frac{\text{Ra}}{2} y^2 - \frac{\text{Ra}}{6})$. Approximating it with the $((P_2)^2, P_1)$ Taylor-Hood element on a coarse mesh as in Figure 1 delivers a velocity error of:

$$\|\nabla \mathbf{u} - \nabla \mathbf{u}_h\| \approx 2.28 \text{Ra}.$$

Since the Rayleigh number in this problem is typically large ($> 10^8$), the Taylor-Hood element (P_2, P_1) is not appropriate for this kind of problem, while the Scott-Vogelius element (P_2, P_1^{disc}) delivers the correct velocity solution $\mathbf{u}_h = \mathbf{0}$. The reason for this different behavior lies in the fact that the velocity solutions of the Taylor-Hood element are not divergence-free. In fact, the L^2 -norm of the divergence of the Taylor-Hood solution in the above problem is $\approx 1.98 \text{Ra}$. The velocity solution of the Scott-Vogelius element is the X -projection $(\langle \mathbf{f}, \mathbf{g} \rangle_X := \int_{\Omega} \nabla \mathbf{f} : \nabla \mathbf{g} \, d\Omega)$ of the Taylor-Hood velocity solution into the subspace of exactly divergence-free velocities. In the terms of Girault and Raviart,

the Taylor-Hood solution delivers an *external approximation* of the above mixed problem, while the Scott-Vogelius solution delivers an internal one ([9], pg. 114). In consequence, for internal approximations the velocity error is completely decoupled from the pressure error, which is not true for external approximations ([9] pg. 116).

There are a number of strategies for avoiding poor mass conservation: several element choices are known to provide pointwise mass conservation [43, 42], discontinuous Galerkin methods typically admit local mass conservation [32] (several in fact deliver pointwise divergence-free solutions [5]), penalization techniques such as grad-div stabilization discussed herein reduce global mass conservation error, and a posteriori methods can be used to enforce the conservation of mass on already computed solutions [25]. For each technique, there are naturally both good features and drawbacks, and therefore a determination of which method is “best” is certainly problem dependent.

Still, in most cases, the use of TH elements with grad-div stabilization is one of the easiest to implement. For many years TH elements have been a popular choice of approximating element in fluid flow simulations, and most downloadable finite element packages have some TH elements implemented. Hence getting a TH code and adding grad-div stabilization is typically convenient and simple. However, until now, it was believed that the improvement in mass conservation using grad-div stabilization, although sometimes significant over usual TH solutions, was limited to an $O(1)$ choice of the stabilization parameter. With this limitation, one had to decide whether the provided mass conservation was good enough, or instead if a different element choice or DG should be used. Hence this work provides a simple solution to correct for poor mass conservation in existing codes, and therefore may lead to TH elements being a good choice on a much wider set of problems. We note that even though in TH approximations, the divergence error is optimally accurate in the asymptotic sense (as $\|\nabla \cdot \mathbf{u}_h\| = \|\nabla \cdot (\mathbf{u}_h - \mathbf{u})\| \leq \sqrt{2} \|\nabla(\mathbf{u}_h - \mathbf{u})\|$), the lack of even local mass conservation makes the approximations unsuitable in modeling some physical problems.

This paper is arranged as follows. In Section 2 we give notation and preliminaries, including a brief discussion of the SV element. In Section 3 we prove that in the cases where SV elements are LBB stable and have optimal approximation properties, grad-div stabilized TH solutions of the NSE converge to SV solutions as the grad-div parameter tends to ∞ . Discussed in Section 4 is the convergence of the TH approximations as $\gamma_n \rightarrow \infty$ on regular meshes. Section 5 presents numerical experiments that illustrate the theory.

2 Preliminaries

We will represent the L^2 norm and inner product by $\|\cdot\|$ and (\cdot, \cdot) , respectively. All other norms used will be clearly denoted with subscripts.

Recall the time dependent incompressible NSE on a polygonal (2d), or polyhedral (3d), domain Ω , and for simplicity with homogeneous Dirichlet boundary conditions:

$$\mathbf{u}_t - \nu \Delta \mathbf{u} + \mathbf{u} \cdot \nabla \mathbf{u} + \nabla p = \mathbf{f}, \quad \text{in } \Omega \times (0, T], \quad (2.1)$$

$$\nabla \cdot \mathbf{u} = 0, \quad \text{in } \Omega \times (0, T], \quad (2.2)$$

$$\mathbf{u}(\mathbf{x}, 0) = \mathbf{u}_0, \quad \text{in } \Omega \quad (2.3)$$

$$\mathbf{u} = \mathbf{0} \quad \text{on } \partial\Omega \times (0, T]. \quad (2.4)$$

Here, \mathbf{u} represents velocity, p the (zero-mean) pressure, \mathbf{f} an external force, and ν the kinematic viscosity.

Throughout the report, $(X_h, Q_h) \subset (H_0^1(\Omega), L_0^2(\Omega))$ will denote either the Taylor-Hood or Scott-Vogelius element pair. For Taylor-Hood elements (X_h, Q_h) are well known to be inf-sup stable. For Scott-Vogelius elements with degree $k \geq d$ and the mesh constructed by a barycenter refinement of a quasi-uniform mesh (details in the following section), or $k = 2$ and $d = 3$ with a Powell-Sabin tetrahedralization, (X_h, Q_h) is inf-sup stable.

The following lemma is used in the analysis below.

Lemma 2.1. *There exists a constant $C^*(\Omega)$, dependent only on the size of Ω , that satisfies $\forall \mathbf{u}, \mathbf{v}, \mathbf{w} \in H_0^1(\Omega)$,*

$$|(\mathbf{u} \cdot \nabla \mathbf{v}, \mathbf{w})| + |((\nabla \cdot \mathbf{u})\mathbf{v}, \mathbf{w})| \leq C^* \|\nabla \mathbf{u}\| \|\nabla \mathbf{v}\| \|\nabla \mathbf{w}\|^{1/2} \|\mathbf{w}\|^{1/2} \quad (2.5)$$

$$|(\mathbf{u} \cdot \nabla \mathbf{v}, \mathbf{w})| + |((\nabla \cdot \mathbf{u})\mathbf{v}, \mathbf{w})| \leq C^* \|\nabla \mathbf{u}\| \|\nabla \mathbf{v}\| \|\nabla \mathbf{w}\| \quad (2.6)$$

Proof. The first inequality follows from Holder's inequality, Ladyzhenskaya inequalities and the Sobolev imbedding theorem. The second follows directly from the first with the Poincaré inequality in $H_0^1(\Omega)$. \square

2.1 Scott-Vogelius and Taylor-Hood elements

The SV element pair is not yet very well known, and so we now give a brief description of it. In essence, the SV pair is the same as the TH pair except that the pressure space is discontinuous and either

- (i) for $k \geq d$, the mesh is a barycenter refinement of a regular mesh, or
- (ii) for $k = 2, d = 3$, the mesh is formed from a barycenter refined mesh by connecting the barycenter nodes (i.e. a Powell-Sabin tetrahedralization).

In short, polynomials of degree k and $k - 1$ are used to approximate the velocity and pressure spaces respectively, and the mesh \mathcal{T}_h that is used must be derived from a regular triangularization (tetrahedralization) of Ω , where each element is refined as stated above. With these mesh constructions, it was proved by Zhang in [42, 44] that the SV elements are LBB stable, and consequently also have optimal approximation properties. It is well known that the TH pair is LBB stable and admits optimal approximation properties for these cases as well [9]. We will restrict our definition of SV elements to these cases where they are LBB stable.

We now formally define the element pairs. In space dimension d , for both TH and SV elements we define X_h to be the space of continuous element-wise vector functions of polynomial order k on \mathcal{T}_h

$$X_h := \left\{ \mathbf{v}_h \in [C(\Omega)]^d : \mathbf{v}_h|_T \in [P_k(T)]^d, \text{ for all } T \in \mathcal{T}_h, \mathbf{v}_h = \mathbf{0} \text{ on } \partial\Omega \right\}.$$

For Taylor-Hood, we define

$$Q_h^{\text{TH}} := \left\{ q_h \in C(\Omega) : q_h|_T \in P_{k-1}, \text{ for all } T \in \mathcal{T}_h, \int_{\Omega} q_h d\Omega = 0 \right\},$$

while the pressure space of the Scott-Vogelius element only differs from Taylor-Hood's in that its pressures are discontinuous:

$$Q_h^{\text{SV}} := \left\{ q_h \in L^2(\Omega) : q_h|_T \in P_{k-1}, \text{ for all } T \in \mathcal{T}_h, \int_{\Omega} q_h d\Omega = 0 \right\}.$$

Note that the dimension of the pressure space for SV elements is significantly larger than that for TH elements. This creates a greater total number of degrees of freedom needed

for linear solves using SV elements, however it is not immediately clear whether this will lead to a significant increase in computational time if preconditioners such as Augmented Lagrangian type are used [2]. The authors plan to consider this question in future studies.

Although the velocity spaces of the TH and SV elements are the same, the spaces of discretely divergence free subspaces are different, and will be denoted by

$$\begin{aligned} V_h^{TH} &:= \{\mathbf{v}_h \in X_h : (\nabla \cdot \mathbf{v}_h, q_h) = 0, \forall q_h \in Q_h^{TH}\}, \\ V_h^{SV} &:= \{\mathbf{v}_h \in X_h : (\nabla \cdot \mathbf{v}_h, q_h) = 0, \forall q_h \in Q_h^{SV}\}. \end{aligned}$$

The SV element is very interesting from the mass conservation point of view since its discrete velocity space and its discrete pressure space fulfill an important property, namely

$$\nabla \cdot X_h \subset Q_h^{SV}. \quad (2.7)$$

Thus, using SV elements, weak mass conservation via

$$(\nabla \cdot \mathbf{u}_h, q_h) = 0, \quad \forall q_h \in Q_h$$

implies strong (pointwise) mass conservation since we can choose the special test function $q_h = \nabla \cdot \mathbf{u}_h$ to get

$$\|\nabla \cdot \mathbf{u}_h\|^2 = 0.$$

In general, the same pressure test function cannot be used in the Taylor-Hood case, since $\nabla \cdot X_h \not\subset Q_h^{TH}$. Hence, in general, approximations obtained using TH elements are not pointwise mass conservative.

2.2 Finite element methods for the NSE

We will study finite element methods for approximating both the steady and time-dependent Navier-Stokes equations. Let $\|\cdot\|_*$ denotes the norm in X^* , the dual space of $X = H_0^1(\Omega)$ endowed with the norm $\|\mathbf{v}\|_X := \|\nabla \mathbf{v}\|$.

For the steady case, we consider the skew symmetrized finite element scheme for the NSE [18]: *Given $\mathbf{f} \in X^*$, find $(\mathbf{u}_h, p_h) \in X_h \times Q_h$, with $Q_h \in \{Q_h^{TH}, Q_h^{SV}\}$ satisfying $\forall (\mathbf{v}_h, q_h) \in X_h \times Q_h$*

$$\begin{aligned} \nu(\nabla \mathbf{u}_h, \nabla \mathbf{v}_h) - (p_h, \nabla \cdot \mathbf{v}_h) + \gamma(\nabla \cdot \mathbf{u}_h, \nabla \cdot \mathbf{v}_h) + (\mathbf{u}_h \cdot \nabla \mathbf{u}_h, \mathbf{v}_h) \\ + \frac{1}{2}((\nabla \cdot \mathbf{u}_h) \mathbf{u}_h, \mathbf{v}_h) = (\mathbf{f}, \mathbf{v}_h), \end{aligned} \quad (2.8)$$

$$(\nabla \cdot \mathbf{u}_h, q_h) = 0, \quad (2.9)$$

where Q_h is either Q_h^{SV} or Q_h^{TH} . Note if $Q_h = Q_h^{SV}$, then trivially $\frac{1}{2}((\nabla \cdot \mathbf{u}_h) \mathbf{u}_h, \mathbf{v}_h) = \gamma(\nabla \cdot \mathbf{u}_h, \nabla \cdot \mathbf{v}_h) = 0$.

The temporal-spatial discretization we study is the Crank-Nicolson Galerkin method, in skew symmetrized form. Denoting $u_h^{n+1/2} := 1/2(u_h^n + u_h^{n+1})$, it is given by:

Given $\mathbf{f} \in X^$, find $(\mathbf{u}_h^{n+1}, \tilde{p}_h^{n+1}) \in X_h \times Q_h$ with $Q_h \in \{Q_h^{TH}, Q_h^{SV}\}$ such that $\forall (\mathbf{v}_h, q_h) \in X_h \times Q_h$ for $n = 0, 1, 2, \dots, M-1$, where $M = T/\Delta t$,*

$$\begin{aligned} \frac{1}{\Delta t}(\mathbf{u}_h^{n+1} - \mathbf{u}_h^n, \mathbf{v}_h) - (\tilde{p}_h^{n+1}, \nabla \cdot \mathbf{v}_h) + \nu(\nabla \mathbf{u}_h^{n+1/2}, \nabla \mathbf{v}_h) + \gamma(\nabla \cdot \mathbf{u}_h^{n+1/2}, \nabla \cdot \mathbf{v}_h) \\ + (\mathbf{u}_h^{n+1/2} \cdot \nabla \mathbf{u}_h^{n+1/2}, \mathbf{v}_h) + \frac{1}{2}((\nabla \cdot \mathbf{u}_h^{n+1/2}) \mathbf{u}_h^{n+1/2}, \mathbf{v}_h) = (\mathbf{f}^{n+1/2}, \mathbf{v}_h) \end{aligned} \quad (2.10)$$

$$(\nabla \cdot \mathbf{u}_h^{n+1}, q_h) = 0. \quad (2.11)$$

Note that \tilde{p}_h^{n+1} is solved for directly, and no initial condition for pressure is required. However, since this is a Crank-Nicolson scheme, \tilde{p}_h^{n+1} approximates $p(t^{n+1/2})$.

We assume the discrete initial velocity, \mathbf{u}_h^0 , is pointwise mass conservative. (There are several stable and optimally accurate ways to ensure this [10, 3], the simplest being to project the initial condition \mathbf{u}^0 into V_h^{SV} .)

Throughout we assume that the discrete approximating system of equations of the time dependent NSE, (2.10)-(2.11), is uniquely solvable. This requires Δt be chosen small enough (dependent on problem data and the meshwidth h , but not on γ). We refer the interested reader to [18, 38] for discussions on the unique solvability of (2.10)-(2.11).

3 Relationship between the Taylor-Hood and the Scott-Vogelius element

Section 2 shows that the Taylor-Hood and the Scott-Vogelius element are not unrelated to each other, as they differ only in their pressure space. But it turns out that much more can be said. For example, it is relatively easy to show that the X -projection of the TH solution to the Stokes problem into the space of divergence free functions is the SV solution of that Stokes problem (independent of grad-div stabilization). However, the results for the NSE are much more interesting.

We prove, under the restrictions where SV elements are LBB stable, that as $\gamma \rightarrow \infty$, the TH solutions to the NSE schemes in Section 2 converge to the SV solution. Roughly speaking, this result can be understood in the following sense: Under the appropriate mesh restrictions discussed above, the grad-div stabilized TH solutions “live between” the TH and SV solutions, which are both LBB stable and have optimal approximation properties. Thus, raising γ significantly larger than $O(1)$ in TH computations can provide excellent mass conservation without “destroying” the solution.

We begin with the steady case.

Theorem 3.1. *Under conditions where SV elements are LBB stable, for any sequence $\{\mathbf{u}_h\}_{\gamma_i}$ of TH velocity solutions to (2.8)-(2.9), there is a subsequence which converges to a SV velocity solution as the grad-div parameter $\gamma_i \rightarrow \infty$. The corresponding sequence of TH “modified pressure” solutions, $\{p_h - \gamma_i \nabla \cdot \mathbf{u}_h\}_{\gamma_i}$, converges to the corresponding SV pressure.*

Moreover, if the SV solution is unique, then the entire sequence converges to the unique SV solution.

Proof. For notational convenience, in the proof we suppress the dependence on h .

We begin with the a priori bound for the steady state approximations, which follows from choosing $\mathbf{v}_h = \mathbf{u}_h$ in (2.8) and $q_h = p_h$ in (2.9) and adding the equations. Recall that for this choice of \mathbf{v}_h , as $(\mathbf{u} \cdot \nabla \mathbf{u}, \mathbf{u}) = 1/2((\nabla \cdot \mathbf{u})\mathbf{u}, \mathbf{u})$ the nonlinearity vanishes. This leaves

$$\nu \|\nabla \mathbf{u}\|^2 + 2\gamma \|\nabla \cdot \mathbf{u}\|^2 \leq \frac{1}{\nu} \|\mathbf{f}\|_*^2 = C(\text{data}), \quad (3.1)$$

where, for the SV approximation, $\|\nabla \cdot \mathbf{u}\| = 0$.

Let $\{\gamma_i\}_{i=1}^\infty \rightarrow \infty$ and \mathbf{u}_i denote the corresponding TH velocity solutions to (2.8)-(2.9). Then, as \mathbf{u}_i is a bounded sequence in a finite dimensional space, we have that there exists $\mathbf{w} \in X_h$ such that a subsequence $\mathbf{u}_{i'} \rightarrow \mathbf{w}$. Again, for notational convenience, we identify the converging subsequence with the entire sequence of Taylor-Hood solutions. From (2.8)-

(2.9) with $\mathbf{v} = \mathbf{u}_i$, $q = p$, we have that

$$\|\nabla \cdot \mathbf{u}_i\| \leq \frac{1}{\gamma_i} (\|\mathbf{f}\|_* \|\nabla \mathbf{u}_i\| + \nu \|\nabla \mathbf{u}_i\|^2) \leq \frac{1}{\gamma_i} C. \quad (3.2)$$

As $\mathbf{u}_{i'} \rightarrow \mathbf{w}$, then $\nabla \cdot \mathbf{u}_{i'} \rightarrow \nabla \cdot \mathbf{w}$, (using the equivalence of norms in a finite dimensional space), and as $\|\nabla \cdot \mathbf{u}_{i'}\| \rightarrow 0$, we have that

$$\|\nabla \cdot \mathbf{w}\| = 0, \quad \text{i.e. } \mathbf{w} \in V_h^{SV}.$$

Next we show that \mathbf{w} is a SV velocity solution. Consider, for $\mathbf{v} \in V_h^{SV}$

$$res(\mathbf{v}) := \nu(\nabla \mathbf{w}, \nabla \mathbf{v}) + (\mathbf{w} \cdot \nabla \mathbf{w}, \mathbf{v}) - (\mathbf{f}, \mathbf{v}). \quad (3.3)$$

Since we are in finite dimensions, the above a-priori estimates imply $\nabla \mathbf{u}_i$, $\nabla \cdot \mathbf{u}_i$, and $\mathbf{u}_i \cdot \nabla \mathbf{u}_i$ are bounded in $L^\infty(\Omega)$. Then, we obtain by the bounded convergence theorem for Lebesgue integration that

$$\begin{aligned} res(\mathbf{v}) &= \nu(\nabla \mathbf{w}, \nabla \mathbf{v}) + (\mathbf{w} \cdot \nabla \mathbf{w}, \mathbf{v}) - (\mathbf{f}, \mathbf{v}) \\ &= \lim_{i \rightarrow \infty} \nu(\nabla \mathbf{u}_i, \nabla \mathbf{v}) + \lim_{i \rightarrow \infty} \gamma_i (\nabla \cdot \mathbf{u}_i, \nabla \cdot \mathbf{v}) + \lim_{i \rightarrow \infty} (\mathbf{u}_i \cdot \nabla \mathbf{u}_i, \mathbf{v}) - (\mathbf{f}, \mathbf{v}) \\ &= \lim_{i \rightarrow \infty} (\nu(\nabla \mathbf{u}_i, \nabla \mathbf{v}) + \gamma_i (\nabla \cdot \mathbf{u}_i, \nabla \cdot \mathbf{v}) + (\mathbf{u}_i \cdot \nabla \mathbf{u}_i, \mathbf{v}) - (\mathbf{f}, \mathbf{v})) \\ &= 0 \end{aligned}$$

holds, since \mathbf{u}_i is a TH solution and satisfies (2.8). Thus \mathbf{w} is a SV velocity solution.

Using the LBB stability of the Scott-Vogelius element on barycentric refined meshes, we get an a-priori bound for $p_i - \gamma_i \nabla \cdot \mathbf{u}_i$ by

$$\|p_i - \gamma_i \nabla \cdot \mathbf{u}_i\| \leq \frac{1}{\beta} \left(\nu \|\nabla \mathbf{u}_i\| + \|\nabla \mathbf{u}_i\|^2 + \|\mathbf{f}\|_* \right),$$

where β is the discrete inf-sup constant of the Scott-Vogelius element.

Similar to the above argument, we obtain that a subsequence of $p_i - \gamma_i \nabla \cdot \mathbf{u}_i$ converges to some \bar{p} and we obtain for all fixed $\mathbf{v} \in X_h$

$$\begin{aligned} (\bar{p}, \nabla \cdot \mathbf{v}) &= \lim_{i \rightarrow \infty} (p_i - \gamma_i \nabla \cdot \mathbf{u}_i, \nabla \cdot \mathbf{v}) \\ &= \lim_{i \rightarrow \infty} (\nu(\nabla \mathbf{u}_i, \nabla \mathbf{v}) + (\mathbf{u}_i \cdot \nabla \mathbf{u}_i, \mathbf{v}) - (\mathbf{f}, \mathbf{v})) \\ &= \nu(\nabla \mathbf{w}, \nabla \mathbf{v}) + (\mathbf{w} \cdot \nabla \mathbf{w}, \mathbf{v}) - (\mathbf{f}, \mathbf{v}) \\ &= (p_{SV}, \nabla \cdot \mathbf{v}). \end{aligned}$$

Since $(Q_h^{TH} + \nabla \cdot X_h) \subset Q_h^{SV}$, we conclude from the LBB condition that $\bar{p} = p_{SV}$. Since the pressure p_{SV} is unique, we further conclude in a classical way that the entire sequence $p_i - \gamma_i \nabla \cdot \mathbf{u}_i$ converges, and not only a subsequence.

Finally, if the SV solution is unique, a simple contradiction argument implies the entire sequence of stabilized Taylor-Hood solutions converges to the SV solution. \square

Next we consider the approximation of the unsteady NSE.

Theorem 3.2. *Any sequence $\{\mathbf{u}_h\}_{\gamma_i}$ of TH velocity solutions to (2.10)-(2.11) converges to the SV velocity solution as the grad-div parameter $\gamma_i \rightarrow \infty$. The corresponding TH “modified pressure” solutions $\{\tilde{p}_h - \gamma_i \nabla \cdot \mathbf{u}_h\}_{\gamma_i}$ converge to the SV pressure solution.*

Proof. We begin again with the a priori bound on the SV and TH solutions, which can be found by choosing the test function $\mathbf{v}_h = \mathbf{u}_h^{n+1/2}$ in (2.10) and $q_h = \tilde{p}_h^{n+1}$ in (2.11), then summing over timesteps: For $0 \leq j \leq M$

$$\begin{aligned} \left\| \mathbf{u}_h^j \right\|^2 + \Delta t \sum_{n=0}^{j-1} \left(\nu \left\| \nabla \mathbf{u}_h^{n+1/2} \right\|^2 + 2\gamma \left\| \nabla \cdot \mathbf{u}_h^{n+1/2} \right\|^2 \right) \\ \leq \frac{\Delta t}{\nu} \sum_{n=0}^{j-1} \left\| \mathbf{f}^{n+1/2} \right\|_*^2 + \left\| \mathbf{u}_h^0 \right\|^2 = C(\text{data}). \end{aligned} \quad (3.4)$$

For the SV solution $\left\| \nabla \cdot \mathbf{u}_h^{n+1/2} \right\| = 0$. The key step for this bound is the vanishing of the nonlinearities for the choice of test function, similar to the steady case.

In addition, by assumption of the existence and uniqueness of the SV solution (which is independent of γ) and LBB stability we have the SV pressure is bounded independent of γ . In particular we have that for $2 \leq j \leq M$

$$\Delta t \sum_{n=0}^{j-1} \left\| \tilde{p}_{SV}^{n+1} \right\|^2 \leq C(\text{data}). \quad (3.5)$$

The key steps for this bound is to majorize the nonlinearity with Holder's inequality, Ladyzhenskaya's inequalities, and Poincaré's inequality, then use that the velocity solution is uniformly bounded in H^1 since we are using a fixed mesh and timestep.

Note that from (3.4) it follows that as $\gamma \rightarrow \infty$, $\nabla \cdot \mathbf{u}_h^{n+1/2} \rightarrow 0$ for $n = 0, \dots, M-1$. Also, as $\nabla \cdot \mathbf{u}_h^0 = 0$, then $\nabla \cdot \mathbf{u}_h^{n+1} \rightarrow 0$ for $n = 0, \dots, M-1$. In addition, as $\left\| \mathbf{u}_h^j \right\|^2$ is uniformly bounded, then the terms $\left\| \nabla \mathbf{u}_h^j \right\|^2$ and $\left\| \nabla \cdot \mathbf{u}_h^j \right\|^2$ are also uniformly bounded. In these later cases the bound will depend upon the mesh parameter h . However, as we are discussing convergence on a fixed mesh, h can be considered a fixed constant.

Let $\mathbf{e} := \mathbf{u}_{SV} - \mathbf{u}_{TH} \in V_h^{TH}$, where $(\mathbf{u}_{SV}, \tilde{p}_{SV})$ and $(\mathbf{u}_{TH}, \tilde{p}_{TH})$ denote the SV and TH solutions respectively. (For convenience, in this proof we suppress the dependence on h .)

For $\mathbf{v} \in V_h^{TH}$, we have that $(\tilde{p}_{TH}^{n+1}, \nabla \cdot \mathbf{v}) = 0$ and thus that

$$\begin{aligned} \frac{1}{\Delta t} (\mathbf{e}^{n+1} - \mathbf{e}^n, \mathbf{v}) - (\tilde{p}_{SV}^{n+1}, \nabla \cdot \mathbf{v}) + \nu (\nabla \mathbf{e}^{n+1/2}, \nabla \mathbf{v}) + \gamma (\nabla \cdot \mathbf{e}^{n+1/2}, \nabla \cdot \mathbf{v}) \\ + (\mathbf{u}_{SV}^{n+1/2} \cdot \nabla \mathbf{u}_{SV}^{n+1/2}, \mathbf{v}) - (\mathbf{u}_{TH}^{n+1/2} \cdot \nabla \mathbf{u}_{TH}^{n+1/2}, \mathbf{v}) + \frac{1}{2} ((\nabla \cdot \mathbf{u}_{SV}^{n+1/2}) \mathbf{u}_{SV}^{n+1/2}, \mathbf{v}) \\ - \frac{1}{2} ((\nabla \cdot \mathbf{u}_{TH}^{n+1/2}) \mathbf{u}_{TH}^{n+1/2}, \mathbf{v}) = \mathbf{0}, \end{aligned} \quad (3.6)$$

which can be written as

$$\begin{aligned} \frac{1}{\Delta t} (\mathbf{e}^{n+1} - \mathbf{e}^n, \mathbf{v}) + \nu (\nabla \mathbf{e}^{n+1/2}, \nabla \mathbf{v}) + \gamma (\nabla \cdot \mathbf{e}^{n+1/2}, \nabla \cdot \mathbf{v}) \\ = -(\mathbf{e}^{n+1/2} \cdot \nabla \mathbf{u}_{SV}^{n+1/2}, \mathbf{v}) - (\mathbf{u}_{TH}^{n+1/2} \cdot \nabla \mathbf{e}^{n+1/2}, \mathbf{v}) - \frac{1}{2} ((\nabla \cdot \mathbf{e}^{n+1/2}) \mathbf{u}_{SV}^{n+1/2}, \mathbf{v}) \\ - \frac{1}{2} ((\nabla \cdot \mathbf{u}_{TH}^{n+1/2}) \mathbf{e}^{n+1/2}, \mathbf{v}) + (\tilde{p}_{SV}^{n+1}, \nabla \cdot \mathbf{v}). \end{aligned} \quad (3.7)$$

With $\mathbf{v} = \mathbf{e}^{n+1/2}$, the identity

$$(\mathbf{u}_{TH}^{n+1/2} \cdot \nabla \mathbf{e}^{n+1/2}, \mathbf{e}^{n+1/2}) + \frac{1}{2} ((\nabla \cdot \mathbf{u}_{TH}^{n+1/2}) \mathbf{e}^{n+1/2}, \mathbf{e}^{n+1/2}) = 0,$$

and using Lemma 2.1, equation (3.7) becomes

$$\begin{aligned}
& \frac{1}{2\Delta t}(\|\mathbf{e}^{n+1}\|^2 - \|\mathbf{e}^n\|^2) + \nu \left\| \nabla \mathbf{e}^{n+1/2} \right\|^2 + \gamma \left\| \nabla \cdot \mathbf{e}^{n+1/2} \right\|^2 \\
&= -\frac{1}{2}((\nabla \cdot \mathbf{e}^{n+1/2}) \mathbf{u}_{SV}^{n+1/2}, \mathbf{e}^{n+1/2}) - (\mathbf{e}^{n+1/2} \cdot \nabla \mathbf{u}_{SV}^{n+1/2}, \mathbf{e}^{n+1/2}) + (\tilde{p}_{SV}^{n+1}, \nabla \cdot \mathbf{e}^{n+1/2}) \\
&\leq C \left\| \nabla \mathbf{e}^{n+1/2} \right\|^2 \left\| \nabla \mathbf{u}_{SV}^{n+1/2} \right\| + \|\tilde{p}_{SV}^{n+1}\| \left\| \nabla \cdot \mathbf{e}^{n+1/2} \right\|. \tag{3.8}
\end{aligned}$$

Since the mesh is fixed, uniform boundedness, equivalence of norms in finite dimensions, and Young's inequality imply

$$\begin{aligned}
& \frac{1}{2\Delta t}(\|\mathbf{e}^{n+1}\|^2 - \|\mathbf{e}^n\|^2) + \nu \left\| \nabla \mathbf{e}^{n+1/2} \right\|^2 + \gamma \left\| \nabla \cdot \mathbf{e}^{n+1/2} \right\|^2 \\
&\leq C \left\| \mathbf{e}^{n+1/2} \right\|^2 + \frac{\gamma}{2} \left\| \nabla \cdot \mathbf{e}^{n+1/2} \right\|^2 + \frac{1}{2\gamma} \|\tilde{p}_{SV}^{n+1}\|^2. \tag{3.9}
\end{aligned}$$

With $\|\mathbf{e}^0\| = 0$, subtracting $\frac{\gamma}{2} \left\| \nabla \cdot \mathbf{e}^{n+1/2} \right\|^2$ from both sides of (3.9), then summing from $n = 0$ to $j - 1$, $2 \leq j \leq M$, we have

$$\begin{aligned}
\|\mathbf{e}^j\|^2 + \Delta t \sum_{n=0}^{j-1} \left(2\nu \left\| \nabla \mathbf{e}^{n+1/2} \right\|^2 + \gamma \left\| \nabla \cdot \mathbf{e}^{n+1/2} \right\|^2 \right) \\
\leq C \Delta t \sum_{n=0}^j \|\mathbf{e}^n\|^2 + \frac{\Delta t}{\gamma} \sum_{n=0}^{j-1} \|\tilde{p}_{SV}^{n+1}\|^2. \tag{3.10}
\end{aligned}$$

The discrete Gronwall inequality [14] then implies that (for Δt sufficiently small)

$$\begin{aligned}
\|\mathbf{e}^j\|^2 + \Delta t \sum_{n=0}^{j-1} \left(2\nu \left\| \nabla \mathbf{e}^{n+1/2} \right\|^2 + \gamma \left\| \nabla \cdot \mathbf{e}^{n+1/2} \right\|^2 \right) &\leq C \frac{\Delta t}{\gamma} \sum_{n=0}^{j-1} \|\tilde{p}_{SV}^{n+1}\|^2 \\
&\leq C \frac{1}{\gamma}.
\end{aligned}$$

Hence, as $\gamma \rightarrow \infty$, $\|\mathbf{e}^j\| \rightarrow 0$, $j = 1, 2, \dots, M$, i.e. $\mathbf{u}_{TH} \rightarrow \mathbf{u}_{SV}$.

With the convergence of the velocity established, we now prove convergence of the modified TH pressure to the SV pressure. Subtracting the TH solution from the SV solution, and using the notation as above, we get $\forall \mathbf{v}_h \in X_h$,

$$\begin{aligned}
& ((\tilde{p}_{TH}^{n+1} - \gamma \nabla \cdot \mathbf{u}_{TH}^{n+1/2}) - \tilde{p}_{SV}^{n+1}, \nabla \cdot \mathbf{v}_h) = \frac{1}{\Delta t} (\mathbf{e}^{n+1} - \mathbf{e}^n, \mathbf{v}_h) + \nu (\nabla \mathbf{e}^{n+1/2}, \nabla \mathbf{v}_h) \\
&+ (\mathbf{e}^{n+1/2} \cdot \nabla \mathbf{u}_{TH}^{n+1/2}, \mathbf{v}_h) + (\mathbf{u}_{SV}^{n+1/2} \cdot \nabla \mathbf{e}^{n+1/2}, \mathbf{v}_h) + \frac{1}{2} ((\nabla \cdot \mathbf{e}^{n+1/2}) \mathbf{u}_{TH}^{n+1/2}, \mathbf{v}_h) + \frac{1}{2} ((\nabla \cdot \mathbf{u}_{SV}^{n+1/2}) \mathbf{e}^{n+1/2}, \mathbf{v}_h) \tag{3.11}
\end{aligned}$$

Now dividing both sides by $\|\nabla \mathbf{v}_h\|$, applying Lemma 2.1 and Cauchy-Schwarz to the right hand side, again using that solutions are uniformly bounded, then reducing, gives

$$\frac{((\tilde{p}_{TH}^{n+1} - \gamma \nabla \cdot \mathbf{u}_{TH}^{n+1/2}) - \tilde{p}_{SV}^{n+1}, \nabla \cdot \mathbf{v}_h)}{\|\nabla \mathbf{v}_h\|} \leq C(\|\mathbf{e}^n\| + \|\mathbf{e}^{n+1}\|). \tag{3.12}$$

Since $(\tilde{p}_{TH}^{n+1} - \gamma \nabla \cdot \mathbf{u}_{TH}^{n+\frac{1}{2}}) \in Q_h^{SV}$ and the restriction on the mesh and k are such that SV elements are LBB stable, the inf-sup condition for (X_h, Q_h^{SV}) implies

$$\left\| (\tilde{p}_{TH}^{n+1} - \gamma \nabla \cdot \mathbf{u}_{TH}^{n+\frac{1}{2}}) - \tilde{p}_{SV}^{n+1} \right\| \leq C(\|\mathbf{e}^n\| + \|\mathbf{e}^{n+1}\|), \quad (3.13)$$

and thus since $\mathbf{e} \rightarrow \mathbf{0}$, we have that

$$\left\| (\tilde{p}_{TH}^{n+1} - \gamma \nabla \cdot \mathbf{u}_{TH}^{n+\frac{1}{2}}) - \tilde{p}_{SV}^{n+1} \right\| \rightarrow 0. \quad (3.14)$$

Note that since it is the time-level $n + \frac{1}{2}$ pressures that are directly solved for in the Crank-Nicolson scheme, it is this convergence result that is relevant, not the n or $n + 1$ time levels. \square

4 Convergence of the TH approximations as $\gamma \rightarrow \infty$ on a regular mesh

In Section 3 we showed that, as the grad-div parameter, γ , goes to infinity the TH velocity approximations converge to the SV velocity approximation. The SV approximation, as described above, requires a barycenter refined mesh. In this section we investigate the question of convergence of the TH approximations as $\gamma \rightarrow \infty$ on a regular mesh. It is known that taking γ too large in the general case can have an over-stabilizing effect [26], although it is also known that with larger γ comes improved mass conservation. Our intention is to further investigate this phenomenon.

4.1 Limiting result

We first show that the approximations converge, and identify the limit function. Analogous to the previous section, it is again a modified pressure that converges to the limit pressure.

We consider the steady-state problem. The extension to the time dependent case is straight-forward, following Section 3. With the notation as introduced above, let

$$V_h^0 := \{v_h \in X_h : \nabla \cdot v_h|_T = 0, \text{ for all } T \in \mathcal{T}_h\}.$$

Note that $V_h^0 \subset V_h^{TH}$ and, under the mesh restrictions so that SV elements are LBB stable, $V_h^0 = V_h^{SV}$.

Let $\mathbf{z}_h \in V_h^0$ be defined by

$$\nu(\nabla \mathbf{z}_h, \nabla \mathbf{v}_h) + (\mathbf{z}_h \cdot \nabla \mathbf{z}_h, \mathbf{v}_h) = (\mathbf{f}, \mathbf{v}_h), \quad \forall \mathbf{v}_h \in V_h^0. \quad (4.1)$$

Since V_h^0 is a closed subspace of $V = \{v \in H_0^1(\Omega), \nabla \cdot v = 0\}$, the Leray-Schauder fixed point theorem can be applied to show solutions to (4.1) exist, in the same way that it is used when the solution and test function space is V (Section 6.3 of [18]). We assume the data is sufficiently small that solutions to (4.1) exist uniquely (e.g. the small data condition given in Section 6.2 of [18]).

Let $r_h \in Q_h^{TH}$ be defined by

$$(r_h, \nabla \cdot \mathbf{v}_h) = \nu(\nabla \mathbf{z}_h, \nabla \mathbf{v}_h) + (\mathbf{z}_h \cdot \nabla \mathbf{z}_h, \mathbf{v}_h) - (\mathbf{f}, \mathbf{v}_h), \quad \forall \mathbf{v}_h \in (V_h^{TH})^\perp, \quad (4.2)$$

where $(V_h^{TH})^\perp$ denotes the orthogonal complement of V_h^{TH} in X_h with respect to the innerproduct $\langle \mathbf{v}, \mathbf{w} \rangle = (\nabla \mathbf{v}, \nabla \mathbf{w})$. In addition, for $\{\mathbf{u}_h\}_{\gamma_i} \in X_h$, let $\rho_{h,i} \in Q_h^{TH}$ be defined by

$$(\rho_{h,i}, \nabla \cdot \mathbf{v}_h) := (\nabla \cdot \mathbf{u}_{h,i}, \nabla \cdot \mathbf{v}_h), \quad \forall \mathbf{v}_h \in (V_h^{TH})^\perp. \quad (4.3)$$

The existence and uniqueness of r_h and $\rho_{h,i}$ follows from (X_h, Q_h^{TH}) satisfying the LBB condition, and the generalized Lax-Milgram theorem.

Theorem 4.1. *For any sequence $\{(\mathbf{u}_h, p_h)\}_{\gamma_i}$ of TH solutions to (2.8)-(2.9) we have that $\{(\mathbf{u}_h, (p_h - \gamma_i \rho_h))\}_{\gamma_i}$ converges to (\mathbf{z}_h, r_h) as the grad-div parameter $\gamma_i \rightarrow \infty$.*

Remark 4.1. *Similar to the limit case for steady NSE in Section 3, if the SV solution is not unique, then a subsequence of TH solutions converges to a SV solution.*

Proof. For notational convenience, in the proof we surpress the dependence on h .

With V_h^{SV} replaced by V_h^0 , the proof that $\{\mathbf{u}_i\} \rightarrow \mathbf{z}$ follows verbatim the proof of Theorem 3.1.

Using the LBB condition, $X_h = V_h^{TH} \oplus (V_h^{TH})^\perp$, and $\mathbf{e}_i = \mathbf{z} - \mathbf{u}_i$

$$\begin{aligned} \beta \|r - (p_i - \gamma_i \rho_i)\| &\leq \sup_{\mathbf{v} \in X_h} \frac{(r, \nabla \cdot \mathbf{v}) - (p_i, \nabla \cdot \mathbf{v}) + (\gamma_i \rho_i, \nabla \cdot \mathbf{v})}{\|\mathbf{v}\|_X} \\ &= \sup_{\mathbf{v} \in (V_h^{TH})^\perp} \frac{(r, \nabla \cdot \mathbf{v}) - (p_i, \nabla \cdot \mathbf{v}) + (\gamma_i \rho_i, \nabla \cdot \mathbf{v})}{\|\nabla \mathbf{v}\|} \\ &= \sup_{\mathbf{v} \in (V_h^{TH})^\perp} \frac{\nu(\nabla \mathbf{e}_i, \nabla \mathbf{v}) + (\mathbf{z} \cdot \nabla \mathbf{z}, \mathbf{v}) - (\mathbf{u}_i \cdot \nabla \mathbf{u}_i, \mathbf{v}) - \frac{1}{2}(\nabla \cdot (\mathbf{u}_i) \mathbf{u}_i, \mathbf{v})}{\|\nabla \mathbf{v}\|} \\ &\leq \nu \|\nabla \mathbf{e}_i\| + \|\mathbf{e}_i \cdot \nabla \mathbf{z}\| + \|\mathbf{u}_i \cdot \nabla \mathbf{e}_i\| + \frac{1}{2} \|\nabla \cdot (\mathbf{e}_i) \mathbf{u}_i\|. \end{aligned}$$

From the boundedness of \mathbf{z} , \mathbf{u}_i , and that $\mathbf{e}_i \rightarrow \mathbf{0}$ as $\gamma_i \rightarrow \infty$, we have that $(p_i - \gamma_i \rho_i) \rightarrow r$. \square

4.2 The dimension of V_h^0

We have that with $\gamma = 0$, the TH approximation lies in V_h^{TH} and with $\gamma = \infty$ the TH approximation lies in V_h^0 . In terms of satisfying the momentum equation, for $\gamma = 0$ the *velocity piece* of the momentum equation is satisfied for all $\mathbf{v} \in V_h^{TH}$, whereas for $\gamma = \infty$ the *velocity piece* of the momentum equation only holds for $\mathbf{v} \in V_h^0$. However, for $\gamma = 0$ the conservation of mass equation is only weakly enforced over Q_h^{TH} , whereas for $\gamma = \infty$ conservation of mass is imposed pointwise.

Clearly, *satisfying* both conservation equations is important. Increasing the value of γ adds additional emphasis to satisfying the conservation of mass equation, while dimenshing the emphasis of satisfying the *velocity piece* of the momentum equation.

Below we investigate the relative dimensions of the spaces V_h^{TH} and V_h^0 for a family of regular meshes, and a family of barycenter refined meshes. Note that for $X_h = [P_2]^2$, only for the barycenter refined mesh do we know that V_h^0 has optimal approximation properties. However, it is interesting to note from Tables 1, 2, that, proportionally, $dim(V_h^0)$ can actually be larger for the regular meshes than the barycenter refined meshes.

Presented in Table 1 are $dim(X_h)$ (assuming homogeneous boundary conditions for the velocity), $dim(V_h^{TH})/dim(X_h)\%$, and $dim(V_h^0)/dim(X_h)\%$ for a sequence of triangulations of the unit square. Table 2 contains the same statistics for a sequence of barycenter

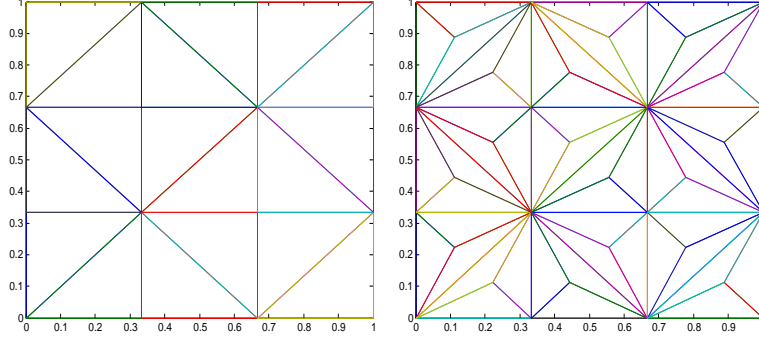


Figure 1: (LEFT) Regular 3×3 triangulation of the unit square; (RIGHT) The 3×3 barycenter refined triangulation of the unit square.

refined meshes. The dimensions of the spaces were computed using the `rank` command in MATLAB. For both triangulations $\dim(V_h^{TH})/\dim(X_h)$ is approximately 87%. The $\dim(V_h^0)/\dim(X_h)$ is slightly higher ($\approx 30\%$) for the regular triangulations than for the barycenter refined triangulations ($\approx 24\%$).

	$\dim(X_h)$	$\dim(Q_h^{TH})$	$\frac{\dim(V_h^{TH})}{\dim(X_h)}\%$	$\frac{\dim(V_h^0)}{\dim(X_h)}\%$
8×8	450	80	82.2	23.8
16×16	1922	288	85.0	27.6
20×20	3042	440	85.5	28.4
28×28	6050	840	86.1	29.2
32×32	7938	1088	86.3	29.5

Table 1: Dimensions of V_h^{TH} and V_h^0 for regular triangulations of the unit square.

	$\dim(X_h)$	$\dim(Q_h^{TH})$	$\frac{\dim(V_h^{TH})}{\dim(X_h)}\%$	$\frac{\dim(V_h^0)}{\dim(X_h)}\%$
4×4	354	56	84.2	18.9
8×8	1474	208	85.9	21.9
12×12	3362	456	86.4	22.9
16×16	6018	800	86.7	23.5
20×20	9442	1240	86.9	23.8

Table 2: Dimensions of V_h^{TH} and V_h^0 for barycenter refined triangulations of the unit square.

5 Numerical Experiments

In this section we investigate the convergence theory of the previous sections. We numerically verify that if the mesh requirements of the theorems are met, then as the grad-div

parameter goes to infinity the TH approximations to NSE converge to the SV approximation.

5.1 Numerical Experiment 1: 2d channel flow around a cylinder on a barycenter refined mesh

The benchmark problem of 2d channel flow around a cylinder has been studied in numerous works, e.g. [34, 16, 17, 19], and is well documented in [34]. The domain is the rectangle $[0, 2.2] \times [0, 0.41]$ representing the channel with flow in the positive x direction, with a circle radius 0.05 centered at $(0.2, 0.2)$ representing the cylinder. No slip boundary conditions are prescribed on the top and bottom of the channel as well as on the cylinder, and the time dependent inflow and outflow velocity profiles are given by

$$\mathbf{u}(0, y, t) = \mathbf{u}(2.2, y, t) = \left[\frac{6}{0.41^2} \sin(\pi t/8) y(0.41 - y), 0 \right]^T, \quad 0 \leq y \leq 0.41.$$

The forcing function is set to zero, $\mathbf{f} = \mathbf{0}$, and the viscosity at $\nu = 0.001$, providing a time dependent Reynolds number, $0 \leq Re(t) \leq 100$. The initial condition is $\mathbf{u} = \mathbf{0}$, and we compute to final time $T = 8$ with time-step $\Delta t = 0.01$.

An accurate approximation of this flow’s velocity field will show a vortex street forming behind the cylinder by $t = 4$, and a fully formed vortex street by $t = 7$. However, there is more than one way to measure accuracy. That is, even if the vortex street forms and the velocity vector field “appears” correct, if the velocity field does not conserve mass, then for many applications the solution may be unacceptable.

Solutions are computed for (P_2, P_1^{disc}) SV elements and for (P_2, P_1) TH elements with $\gamma = 0, 1, 100, 10,000$, all on the same barycenter refined mesh of a Delauney triangulation. This provides 6,578 velocity degrees of freedom, dof, and 4,797 pressure dof for the SV pressure, and 845 pressure degrees of freedom for the TH simulation. Results of these simulations are shown in Table 3, and Figures 2 and 3.

γ	$\ \nabla \mathbf{u}_{TH}^\gamma(t=7) - \nabla \mathbf{u}_{SV}(t=7)\ $
0	5.7086
1	0.7616
100	7.9856e-3
10,000	8.5311e-5

Table 3: The table above shows convergence of the grad-div stabilized TH approximations to the SV approximation for Numerical Experiment 1.

Table 3 shows convergence of the TH approximations to the SV approximation as $\gamma \rightarrow \infty$. This agrees with the theory of Section 3. Figure 2 shows the plots of the velocity field, speed contours and pressure contours for SV and TH approximations with $\gamma = 0, 1, 100, 10,000$. The convergence as γ gets large of the TH approximations to the SV approximation is clear.

The benefit to mass conservation of increasing γ is shown in Figure 3. Here we see with $\gamma = 10,000$, excellent mass conservation is achieved. Also we note that for the unstabilized TH approximation, $\|\nabla \cdot \mathbf{u}_h^n\| = O(1)$.

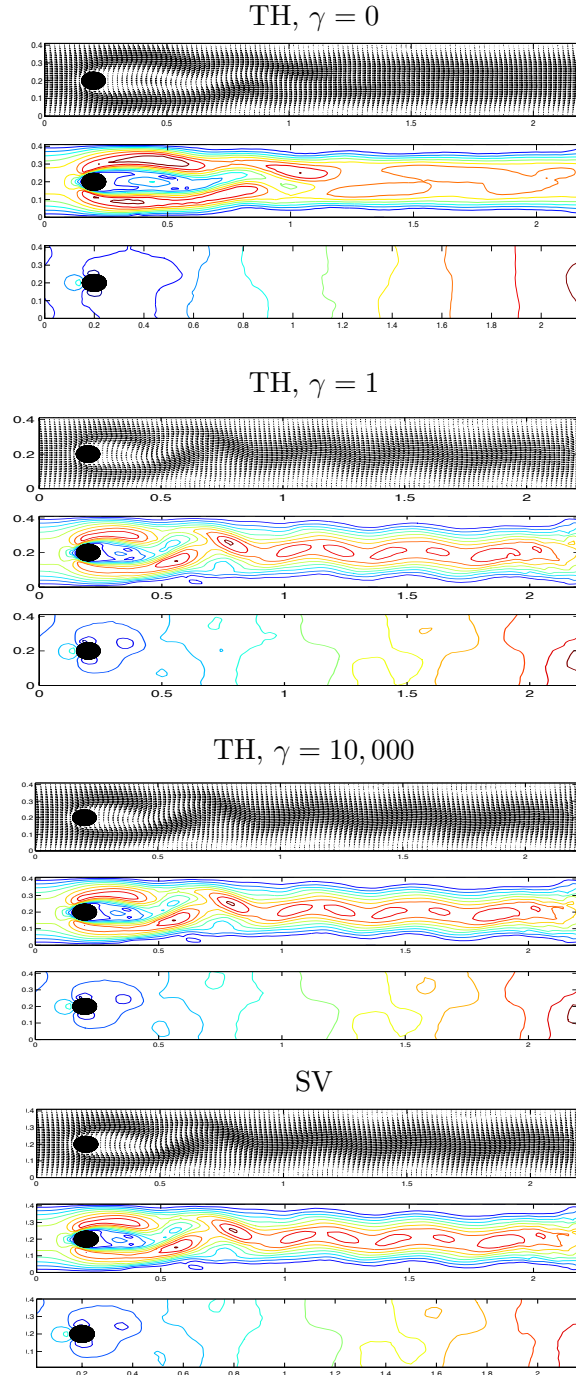


Figure 2: The $t=7$ velocity fields, speed contours, and pressure contour plots for approximations obtained using TH elements without grad-div stabilization (top), TH elements with $\gamma = 1$ (second from top), TH elements with $\gamma = 10,000$ (third from top), and the SV element approximation (bottom), on a barycentric mesh and $k = 2$. Convergence to the SV approximation as γ increases is clear. The SV and TH with $\gamma = 10,000$ approximations are nearly indistinguishable and agree well with known results [34, 16, 17]. Some slight differences with these and the plotted solution for TH elements with $\gamma = 1$ can be seen in the speed contours, and the $\gamma = 0$ solution is clearly underresolved.

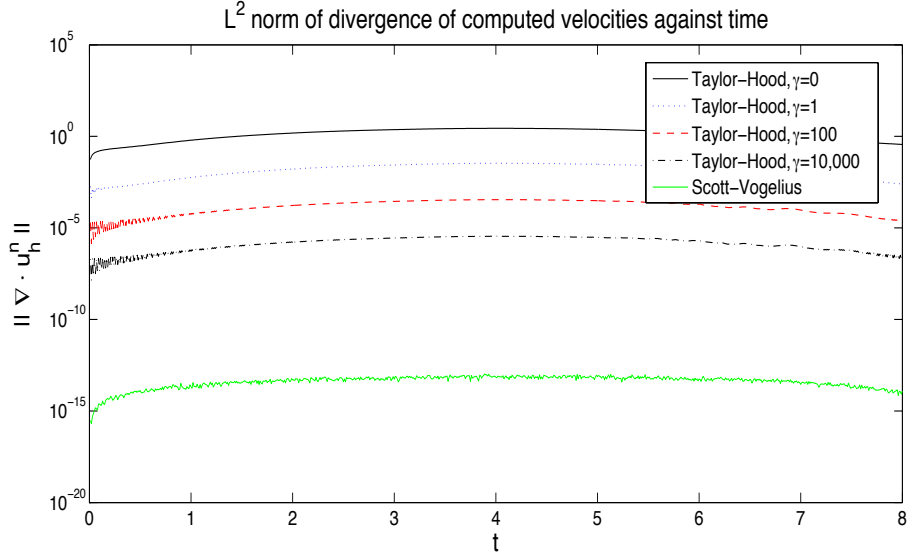


Figure 3: Shown above are the plots of $\|\nabla \cdot \mathbf{u}_h^n\|$ vs. time for the SV and TH approximations for Numerical Experiment 1, with varying γ .

5.2 Numerical Experiment 2: 2d flow around a cylinder on a regular mesh

For our next experiment, we investigate the effect of large γ with TH elements ($k = 2$) on a regular mesh (Delauney triangulation). We proved in Section 4 that velocity solutions converge as $\gamma \rightarrow \infty$. Illustrated in Figure 4 are TH solutions corresponding to $\gamma = 0, 1, 100, 10,000$, using a mesh with 7,414 velocity degrees of freedom and 915 pressure degrees of freedom. This mesh is somewhat finer than in Experiment 1, and we see in the plot of the solution in Figure 4 that the $\gamma = 0$ solution has a more resolved velocity field than the $\gamma = 0$ solution of Experiment 1.

From Figure 4, we note that as γ increases, the solutions appear to converge, in agreement with the theory. Conservation of mass improves in the same manner as in Experiment 1 on the barycenter refined mesh (plot omitted).

5.3 Numerical Experiment 3: The 3d driven cavity on a barycenter refined mesh

We next consider the benchmark problem of the 3d lid-driven cavity. This problem has been well-studied, [41, 27], and the description is as follows. The domain Ω is the $(-1, 1)^3$ cube, for boundary conditions the top of the box (lid) is prescribed the velocity $\mathbf{u} = [1, 0, 0]^T$ with the velocity on the the sides and bottom set to zero ($\mathbf{u} = \mathbf{0}$), and the viscosity $\nu = 1/50$, giving the Reynolds' number $Re = 2 \cdot 1 \cdot 50 = 100$. We compute with a barycenter refinement of a uniform tetrahedral mesh, consisting of 51,119 total dof for the (P_3, P_2) TH elements (46,038 velocity and 5,081 pressure) and 76,038 total dof for (P_3, P_2^{disc}) SV elements (46,038 velocity and 30,000 pressure). The problem is solved directly for the steady state approximation with a Newton iteration, using as the initial guess $\mathbf{u}(\mathbf{x}) = \mathbf{0}$, $\mathbf{x} \in \Omega$. Five iterations were required to converge to a tolerance of 10^{-10} for each of the tests.

We compare the SV approximation and TH approximations with stabilization param-

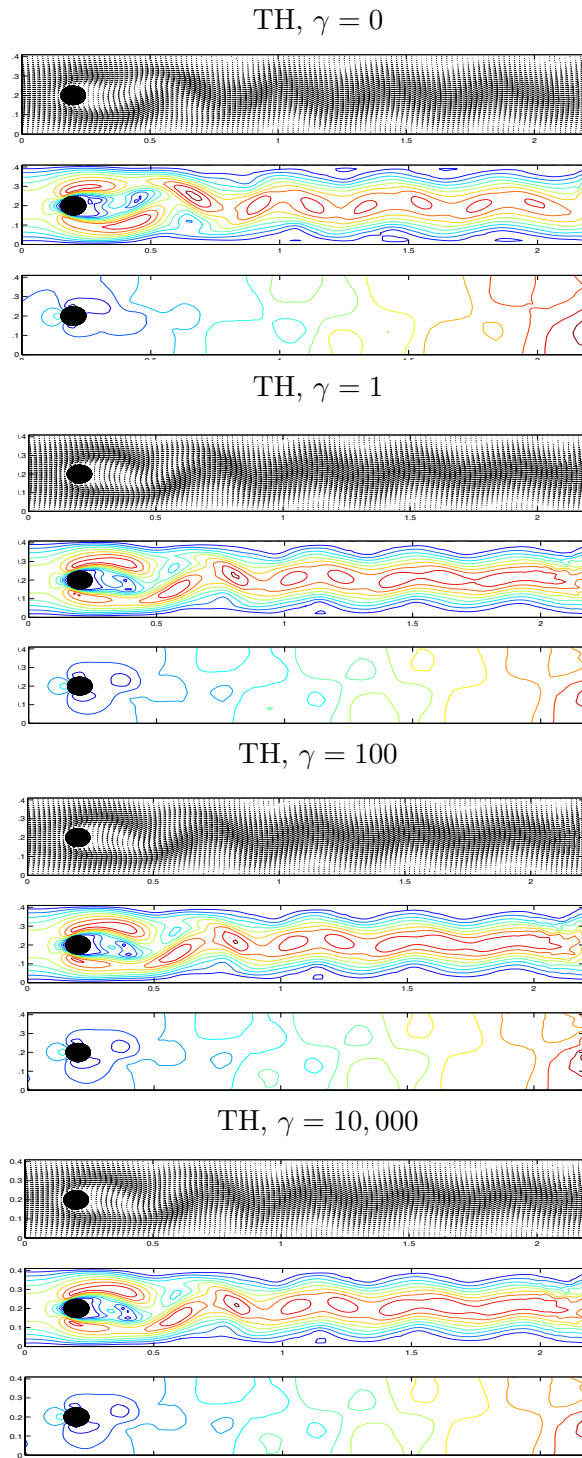


Figure 4: The $t=7$ velocity fields, speed contours, and pressure contour plots for solutions obtained using TH elements without grad-div stabilization (TOP), TH elements with $\gamma = 1$, $\gamma = 100$, and $\gamma = 10,000$ (BOTTOM), using a general (non-barycentric) mesh.

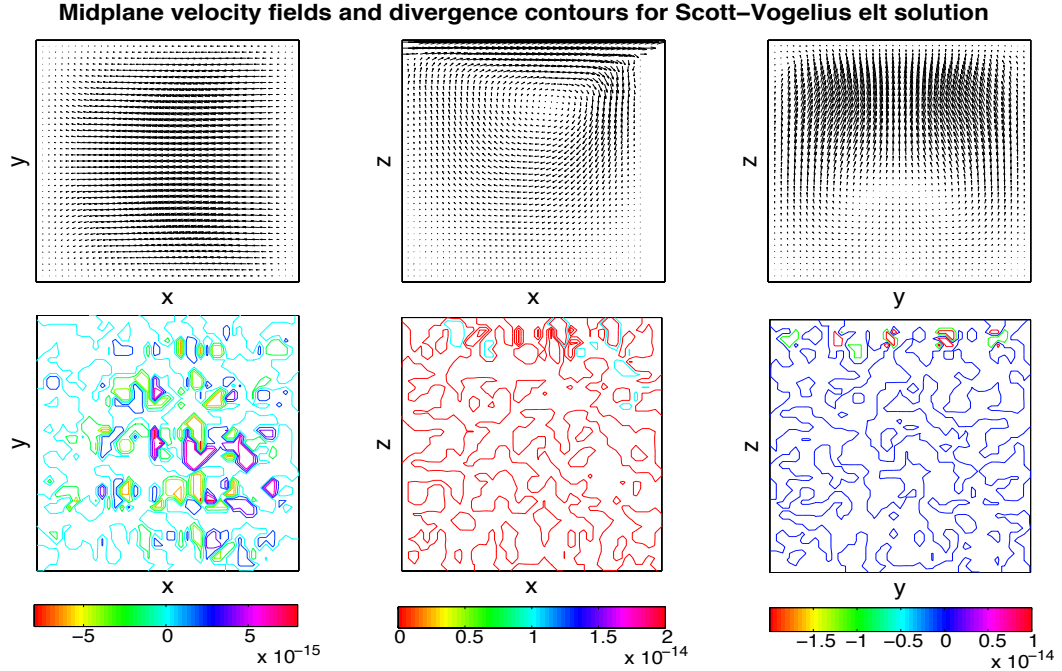


Figure 5: Velocity profiles and divergence contours for mid-sliceplanes, for the lid-driven cavity problem with SV elements. Pointwise mass conservation is observed.

eters $\gamma = 0, 1, 100, 10,000$. Plots of the TH ($\gamma = 0$) and SV approximations' midplane velocity vector fields and divergence contours are presented in Figures 5-6. A visual inspection of the velocity fields indicates they appear the same, and in agreement with the known solution [41]. However, the divergence contours show these solutions are in fact quite different. While the SV solution conserves mass up to roundoff error, the TH solution has $O(1)$ mass conservation in the upper corners, and thus has poor physical accuracy. For the TH approximations using grad-div stabilization, we observe the velocity vector fields look identical to TH and SV plots as in Figures 5 and 6, and the magnitude of the divergence contours decreases as γ increases (pictures omitted).

The convergence of the TH velocity approximations to the SV velocity approximation is shown in Table 4, giving verification to the theory of Section 3. Also shown in this table is the improvement in mass conservation from raising γ .

γ	$\ \nabla \mathbf{u}_{TH}^\gamma - \nabla \mathbf{u}_{SV}\ $	$\ \nabla \cdot \mathbf{u}_{TH}^\gamma\ $
0	1.0653	4.601E-1
1	0.2093	5.409E-2
100	0.0029	7.056E-4
10,000	2.951E-5	7.081E-6

Table 4: Convergence of the grad-div stabilized TH approximations toward the SV approximation as $\gamma \rightarrow \infty$ for the $Re = 100$ 3d driven cavity problem.

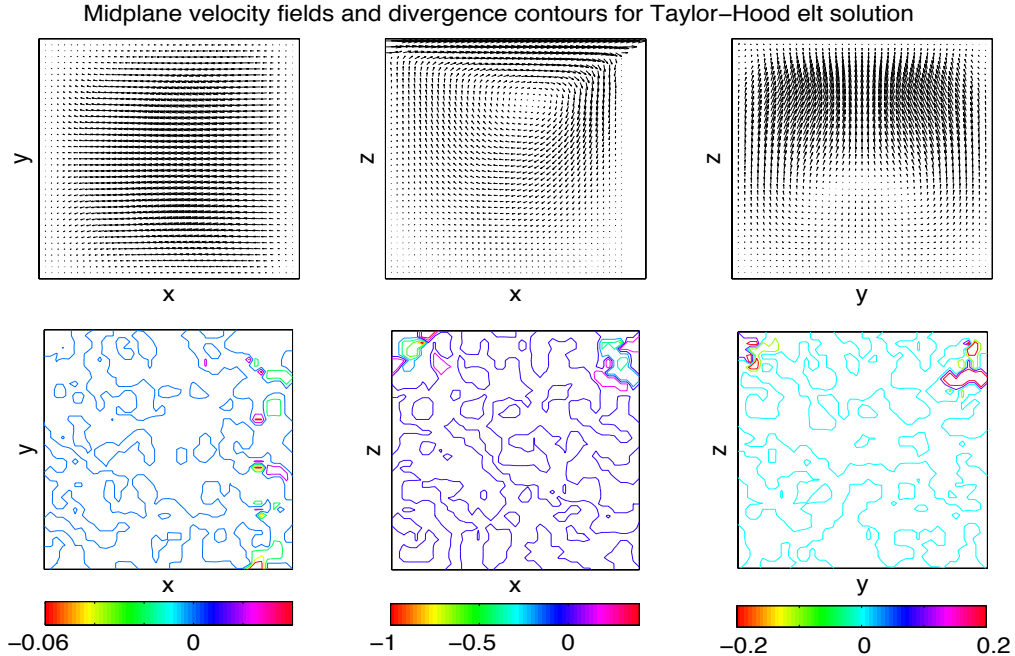


Figure 6: Velocity profiles and divergence contours for mid-sliceplanes, for the lid-driven cavity problem with TH elements and $\gamma = 0$. Very poor mass conservation is observed.

5.4 Numerical Experiment 4: The 3d driven cavity on a regular mesh

In 3d, the (P_2, P_1) TH element is a popular approximation choice. The theory we developed in Section 4 shows that as γ becomes large (assuming exact arithmetic) the velocity approximations converge to a pointwise mass conservative solution $\mathbf{z}_h \in V_h^0$.

We compute solutions to the $\text{Re}=100$ 3d driven cavity problem studied in numerical experiment 3, with (P_2, P_1) TH elements on a uniform mesh and 29,114 total dof, using $\gamma = 0$ and $\gamma = 10,000$. Sliceplanes of the solutions are shown in Figure 7, and while we see that the $\gamma = 0$ solution appears correct and matches the solutions from numerical experiment 3, the solution with $\gamma = 10,000$ appears to be visibly worse: while the xz midplane appears close to accurate, the xy and yz midplane plots are both visibly inaccurate. As expected, mass conservation is significantly improved for larger γ ,

$$\|\nabla \cdot u_h^{\gamma=10,000}\| = 4.394E - 5, \quad \|\nabla \cdot u_h^{\gamma=0}\| = 3.7634E - 1.$$

We remark that, for this mesh, the added emphasis ($\gamma = 10,000$) on conservation of mass occurs at the detriment of the conservation of momentum and, consequently, the flow field.

5.5 Numerical Experiment 5: Optimal γ

Recent work with grad-div stabilization suggests that the optimal γ for many problems is $O(1)$ [29, 28, 19, 20, 26]. While we do not contest this conjecture, we suggest $O(1)$ should instead be a starting point to finding an optimal γ . Experiment 1 illustrates a problem

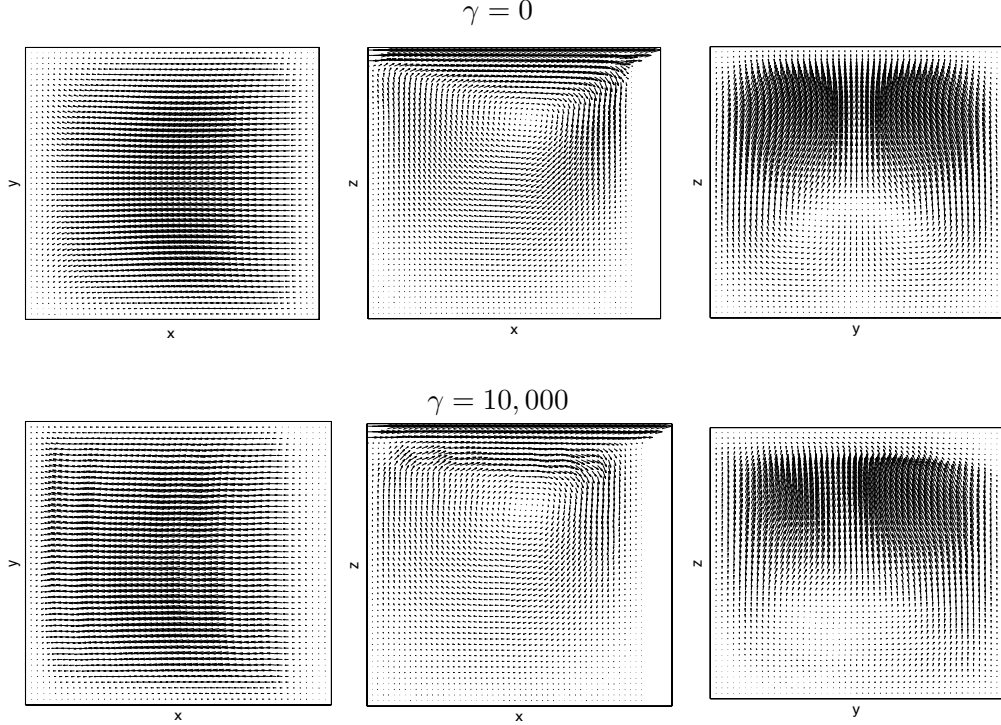


Figure 7: Velocity profiles for mid-sliceplanes, for the lid-driven cavity problem with (P_2, P_1) elements, with $\gamma = 0$ (TOP) and $\gamma = 10,000$ (BOTTOM), for numerical experiment 4.

where γ large gave excellent results. For Experiment 4, γ large ($\gg O(1)$) lead to an unsatisfactory deterioration in the approximation of the flow field. Additionally, what one considers an optimal γ can change depending on criteria. Specifically, if mass conservation is important (as it often is) and a computed solution's incompressibility (or lack thereof) is considered, e.g. if the $H(\text{div})$ norm is used instead of L^2 , then an optimal value of γ can change significantly. Recall the $H(\text{div})$ norm is defined by

$$\|\phi\|_{H(\text{div})} := \sqrt{\|\phi\|^2 + \|\nabla \cdot \phi\|^2}.$$

The setup for this experiment is as follows: Using the selected NSE solution

$$u = \begin{pmatrix} 2x^2(x-1)^2y(2y-1)(y-1) \\ -2x(x-1)(2x-1)y^2(y-1)^2 \end{pmatrix}, \quad p = \sin(x),$$

on the unit square domain with $\nu = 0.0001$, $h = 1/16$ (regular mesh), solutions were computed using (P_2, P_1) TH elements and varying values of the parameter γ . The computed solution was then compared to the true solution, and the L^2 and $H(\text{div})$ norms of the error were calculated. Results are given in Table 5, and show that the optimal γ for minimizing the L^2 and H^1 velocity error is $O(1)$. However, for the $H(\text{div})$ velocity and the L^2 pressure errors, the optimal γ is significantly larger. In fact, the $H(\text{div})$ velocity error for the $\gamma = 100$ solution is less than half of that for $\gamma = O(1)$.

γ	$\ \mathbf{u}_{TH}^\gamma - \mathbf{u}_{true}\ $	$\ \mathbf{u}_{TH}^\gamma - \mathbf{u}_{true}\ _{H^1}$	$\ \mathbf{u}_{TH}^\gamma - \mathbf{u}_{true}\ _{H(div)}$	$\ p_{TH}^\gamma - p_{true}\ $
0	6.61E-2	3.28E-1	2.99E-1	8.5010E-5
0.1	5.53E-5	4.50E-3	4.77E-4	7.3178E-5
1	2.67E-5	2.12E-3	5.78E-5	7.3165E-5
10	2.72E-5	2.15E-3	2.77E-5	7.3165E-5
100	2.73E-5	2.16E-3	2.73E-5	7.3165E-5
1,000	2.73E-5	2.16E-3	2.73E-5	7.3164E-5
10,000	2.73E-5	2.16E-3	2.73E-5	7.3164E-5
100,000	2.73E-5	2.16E-3	2.73E-5	7.3164E-5

Table 5: L^2 , H^1 and $H(div)$ velocity errors and L^2 pressure error for various stabilization parameters for Numerical Experiment 5.

6 Conclusions and Future Directions

We have proven and illustrated numerically that under some mild restrictions, for the Navier-Stokes problem as the grad-div stabilization parameter, γ , goes to ∞ the TH approximations ($k \geq d$) on a barycenter refined mesh converge to the SV approximation. On a regular mesh we have proven that the TH approximations converge to a pointwise divergence-free solution as $\gamma \rightarrow \infty$.

Little effort is needed to incorporate grad-div stabilization into an existing finite element approximation of the NSE. Also, due to the similarity of Taylor-Hood elements and Scott-Vogelius elements, many existing codes using Taylor-Hood elements can be easily converted to use Scott-Vogelius elements (provided the mesh is created appropriately). Hence the methods discussed in this paper may be of significant interest to engineers and fluid dynamicists interested in better mass conservation with reasonable development cost.

The “optimal” choice for γ is an interesting and open question. In [26, 8] Olshanskii et al. investigated optimal values for γ . In [26], they remarked “... the search of an optimal γ as a trade-off between mass and energy balance in the FE system.” From their investigations, they found that an optimal value of $\gamma \in [0.1, 1.0]$ was optimal for minimizing the L^2 and H^1 errors in the TH approximations. Note that for $\gamma = O(1)$ in the numerical examples presented in Section 5 the TH approximations gave large divergence error, which for many physical problems would be unacceptable. If so, a more appropriate physical criteria for determining an optimal value for γ may be to minimize the error in the $H(div)$ norm, or to determine γ which minimizes the H^1 error subject to $\|\nabla \cdot (\mathbf{u}_h)\| < tol$. We plan to investigate appropriate choices for γ in subsequent work.

References

- [1] D.N. Arnold and J. Qin. Quadratic velocity/linear pressure Stokes elements. In R. Vichnevetsky, D. Knight, and G. Richter, editors, *Advances in Computer Methods for Partial Differential Equations VII*, pages 28–34. IMACS, 1992.
- [2] M. Benzi, M. Olshanskii, and Z. Wang. Modified augmented Lagrangian preconditioners for the incompressible Navier-Stokes equations. *International Journal for Numerical Methods in Fluids*, to appear, 2010.

- [3] P. Bochev and M. Shashkov. Constrained interpolation (remap) of divergence-free fields. *Comput. Methods Appl. Mech. Engrg.*, 194:511–530, 2005.
- [4] F. Brezzi and M. Fortin. *Mixed and Hybrid Finite Element Methods*. Springer-Verlag, 1991.
- [5] B. Cockburn, G. Kanschat, and D. Schötzau. A note on discontinuous Galerkin divergence-free solutions of the Navier-Stokes equations. *J. Sci. Comput.*, 31(1-2):61–73, 2007.
- [6] H. Elman, D. Silvester, and A. Wathen. *Finite Elements and Fast Iterative Solvers with Applications in Incompressible Fluid Dynamics*. Numerical Mathematics and Scientific Computation. Oxford University Press, Oxford, 2005.
- [7] S. Ganesan and V. John. Pressure separation — A technique for improving the velocity error in finite element discretisations of the Navier-Stokes equations. *Appl. Math. Comp.*, 165(2):275–290, 2005.
- [8] T. Gelhard, G. Lube, M.A. Olshanskii, and J.-H. Starcke. Stabilized finite element schemes with LBB-stable elements for incompressible flows. *J. Comput. Appl. Math.*, 177:243–267, 2005.
- [9] V. Girault and P.-A. Raviart. *Finite Element Methods for Navier-Stokes equations : Theory and Algorithms*. Springer-Verlag, 1986.
- [10] V. Girault and L. R. Scott. A quasi-local interpolation operator preserving the discrete divergence. *Calcolo*, 40:1–19, 2003.
- [11] P. Gresho and R. Sani. *Incompressible Flow and the Finite Element Method*, volume 2. Wiley, 1998.
- [12] M. Gunzburger. *Finite Element Methods for Viscous Incompressible Flow: A Guide to Theory, Practice, and Algorithms*. Academic Press, Boston, 1989.
- [13] J. Heywood and R. Rannacher. Finite element approximation of the nonstationary Navier-Stokes problem. I. Regularity of solutions and second-order error estimates for spatial discretization. *SIAM Journal on Numerical Analysis*, 19(2):275–311, 1982.
- [14] J. Heywood and R. Rannacher. Finite element approximation of the nonstationary Navier-Stokes problem. Part IV: Error analysis for the second order time discretization. *SIAM J. Numer. Anal.*, 2:353–384, 1990.
- [15] V. John. *Large Eddy Simulation of Turbulent Incompressible Flows. Analytical and Numerical Results for a Class of LES Models*”, volume 34 of *Lecture Notes in Computational Science and Engineering*. Springer-Verlag Berlin, Heidelberg, New York, 2004.
- [16] V. John. Reference values for drag and lift of a two dimensional time-dependent flow around a cylinder. *International Journal for Numerical Methods in Fluids*, 44:777–788, 2004.
- [17] A. Labovsky, W. Layton, C. Manica, M. Neda, and L. Rebholz. The stabilized extrapolated trapezoidal finite element method for the Navier-Stokes equations. *Comput. Methods Appl. Mech. Engrg.*, 198:958–974, 2009.

- [18] W. Layton. *An Introduction to the Numerical Analysis of Viscous Incompressible Flows*. SIAM, 2008.
- [19] W. Layton, C. Manica, M. Neda, M.A. Olshanskii, and L. Rebholz. On the accuracy of the rotation form in simulations of the Navier-Stokes equations. *J. Comput. Phys.*, 228(5):3433–3447, 2009.
- [20] W. Layton, C. Manica, M. Neda, and L. Rebholz. Numerical analysis and computational comparisons of the NS-omega and NS-alpha regularizations. *Comput. Methods Appl. Mech. Engrg.*, 199:916–931, 2010.
- [21] A. Linke. *Divergence-free mixed finite elements for the incompressible Navier-Stokes Equation*. PhD thesis, University of Erlangen, 2007.
- [22] A. Linke. Collision in a cross-shaped domain — A steady 2d Navier-Stokes example demonstrating the importance of mass conservation in CFD. *Comp. Meth. Appl. Mech. Eng.*, 198(41–44):3278–3286, 2009.
- [23] G. Matthies and L. Tobiska. Mass conservation of finite element methods for coupled flow-transport problems. In G. Lube and G. Rapin, editors, *Proceedings of the International Conference on Boundary and Interior Layers*. BAIL, 2006.
- [24] A. Münch and B. Wagner. Galerkin method for feedback controlled Rayleigh-Bénard convection. *Nonlinearity*, 21(11):2625–2651, 2008.
- [25] I.M. Navon. Implementation of a posteriori methods for enforcing conservation of potential enstrophy and mass in discretized shallow water equation models. *Monthly Weather Review*, 109:946–958, 1981.
- [26] M. Olshanskii, G. Lube, T. Heister, and J. Löwe. Grad-div stabilization and subgrid pressure models for the incompressible Navier-Stokes equations. *Comp. Meth. Appl. Mech. Eng.*, 198:3975–3988, 2009.
- [27] M. Olshanskii and L. Rebholz. Velocity-Vorticity-Helicity formulation and a solver for the Navier-Stokes equations. *Journal of Computational Physics*, 229(11):4291–4303, 2010.
- [28] M.A. Olshanskii. A low order Galerkin finite element method for the Navier-Stokes equations of steady incompressible flow: A stabilization issue and iterative methods. *Comp. Meth. Appl. Mech. Eng.*, 191:5515–5536, 2002.
- [29] M.A. Olshanskii and A. Reusken. Navier-Stokes equations in rotation form: a robust multigrid solver for the velocity problem. *SIAM J. Sci. Comput.*, 23:1682–1706, 2002.
- [30] M.A. Olshanskii and A. Reusken. Grad-Div stabilization for the Stokes equations. *Math. Comp.*, 73:1699–1718, 2004.
- [31] J. Qin. *On the convergence of some low order mixed finite elements for incompressible fluids*. PhD thesis, Pennsylvania State University, 1994.
- [32] B. Riviere. *Discontinuous Galerkin Methods for Solving Elliptic and Parabolic Equations: Theory and Implementation*. SIAM, 2008.

- [33] H.-G. Roos, M. Stynes, and L. Tobiska. *Robust Numerical Methods for Singularly Perturbed Differential Equations*, volume 24 of *Springer Series in Computational Mathematics*. Springer, Berlin, 2nd edition, 2008.
- [34] M. Schäfer and S. Turek. The benchmark problem ‘flow around a cylinder’ flow simulation with high performance computers II. in *E.H. Hirschel (Ed.), Notes on Numerical Fluid Mechanics*, 52, Braunschweig, Vieweg:547–566, 1996.
- [35] L.R. Scott and M. Vogelius. Conforming finite element methods for incompressible and nearly incompressible continua. In *Large-scale computations in fluid mechanics, Part 2*, volume 22-2 of *Lectures in Applied Mathematics*, pages 221–244. Amer. Math. Soc., 1985.
- [36] L.R. Scott and M. Vogelius. Norm estimates for a maximal right inverse of the divergence operator in spaces of piecewise polynomials. *Mathematical Modelling and Numerical Analysis*, 19(1):111–143, 1985.
- [37] H. Sohr. *The Navier-Stokes Equations, An Elementary Functional Analytic Approach*. Birkhäuser Advanced Texts. Birkhäuser Verlag Basel, Boston, Berlin, 2001.
- [38] R. Temam. *Navier-Stokes Equations : Theory and Numerical Analysis*. Elsevier North-Holland, 1979.
- [39] M. Vogelius. An analysis of the p -version of the finite element method for nearly incompressible materials. uniformly valid, optimal error estimates. *Numer. Math.*, 41:39–53, 1983.
- [40] M. Vogelius. A right-inverse for the divergence operator in spaces of piecewise polynomials. Application to the p -version of the finite element method. *Numer. Math.*, 41:19–37, 1983.
- [41] K.L. Wong and A.J. Baker. A 3d incompressible Navier-Stokes velocity-vorticity weak form finite element algorithm. *International Journal for Numerical Methods in Fluids*, 38:99–123, 2002.
- [42] S. Zhang. A new family of stable mixed finite elements for the 3d Stokes equations. *Math. Comp.*, 74(250):543–554, 2005.
- [43] S. Zhang. A family of $Q_{k+1,k} \times Q_{k,k+1}$ divergence-free finite elements on rectangular grids. *SIAM J. Numer. Anal.*, 47(3):2090–2107, 2009.
- [44] S. Zhang. Quadratic divergence-free finite elements on Powell-Sabin tetrahedral grids. *Submitted*, Available as technical report at <http://www.math.udel.edu/~szhang/>, 2010.